



## Determination of the maximal singularity-free orientation workspace for the Gough–Stewart platform

Qimi Jiang, Clément M. Gosselin \*

Department of Mechanical Engineering, Laval University, Pavillon Adrien-Pouliot, 1065 Avenue de la Médecine, Québec City, QC, Canada G1V 0A6

### ARTICLE INFO

*Article history:*

Received 24 November 2007

Received in revised form 13 July 2008

Accepted 14 July 2008

Available online 20 September 2008

*Keywords:*

Gough–Stewart platform

Roll–Pitch–Yaw angles

Workspace surface

Maximal singularity-free orientation workspace

### ABSTRACT

This work addresses the determination of the maximal singularity-free orientation workspace at a prescribed position of the Gough–Stewart platform. Using the Roll–Pitch–Yaw angles ( $\phi, \theta, \psi$ ), the orientation workspace at a prescribed position can be defined by up to 12 workspace surfaces. A numerical algorithm is developed to determine these 12 workspace surfaces in order to obtain the maximal singularity-free orientation workspace as well as the corresponding leg length ranges. Besides, to compare the maximal singularity-free orientation workspace with the maximal singularity-free sphere, an iterative algorithm for determining the maximal singularity-free sphere is also provided.

© 2008 Elsevier Ltd. All rights reserved.

### 1. Introduction

Parallel mechanisms possess significant advantages over serial mechanisms in terms of dynamic properties, load-carrying capacity, high accuracy as well as stiffness or stability. They are widely used as flight and vehicle simulators, high-precision machining centres, mining machines, motion simulators and so on. 复杂的运动轨迹 [1–10]

However, the closed-loop nature of their architectures limits the motion of the platform and creates complex kinematic singularities inside the workspace [1–10]. Hence, to maximize the singularity-free workspace of parallel mechanisms is highly desirable for robot designers. 提高工作空间 + 避开奇异点 [1–16]

The definition of the position workspace as well as its singularity analysis is relatively simple and straightforward. So far, most research work has just focused in this area [1–16].

However, the definition of the orientation workspace is more complex. Its representation has been a challenging task. Especially, the orientation workspace can be defined by numerous parameterization approaches such as the Roll–Pitch–Yaw angles, the direction cosine matrix (DCM), Euler axis and angle (rotation vector), Euler angles, tilt and torsion angles [17], quaternions, Rodrigues parameters as well as Cayley–Klein parameters. Even for Euler angles, there are 12 possible conventions. So far, very few works exist on the topic of orientation workspace computation. The relevant works in this area may be found in [15–22]. 相关工作空间 [15–22]

A pencil of rays from the origin was used in [16] to compute the orientation workspace. Obviously, the computation precision depends on the density of the used rays and details about this point were not provided. However, the main drawback can be that with this approach, it is difficult to obtain the complete boundary of the real orientation workspace because the shape of the orientation workspace in most cases is very complex.

\* Corresponding author. Tel.: +1 418 656 3474; fax: +1 418 656 7415.

E-mail addresses: [qimi.jiang.1@ulaval.ca](mailto:qimi.jiang.1@ulaval.ca) (Q. Jiang), [gosselin@gmc.ulaval.ca](mailto:gosselin@gmc.ulaval.ca) (C.M. Gosselin).

仅用两个量  $t_1, t_2$  表示  $B_i$

Considering the complexity of the orientation workspace, only two of the three possible rotations of the end-effector of the Gough–Stewart platforms were computed and represented in [18,19]. In [18], the rotation around the unit normal of the platform was set to 0. Hence, the remaining 2D rotations of the platform lead to the locus of the unit normal of the platform being an inverted hollow pyramid. This pyramid was referred to as the orientation pyramid. Then, the area of all the facets of the orientation pyramid was used as the measure of the orientation workspace.

Similarly, a unit link (a link with unit length) on the platform was used in [19] to describe the orientation workspace. One end of the chosen unit link is the fixed point. When the platform rotates around the fixed point, the locus of the other end of the chosen unit link is a patch of spherical surface. Then, the area of the obtained patch of spherical surface was used as the measure of the orientation workspace. As pointed out in [19], this algorithm is able to determine only two of the three possible rotations of the end-effector. Obviously, the rotation around the chosen unit link was neglected.

To the best of the authors' knowledge, the maximal singularity-free orientation workspace has not yet addressed because of its complexity. Instead, a maximal singularity-free sphere was used in [10] as a measure of the maximal singularity-free orientation workspace. However, any orientation workspace cannot be a sphere in practice.

This work focuses on the determination of the 3D maximal singularity-free orientation workspace of the Gough–Stewart platform using the Roll–Pitch–Yaw angles ( $\phi, \theta, \psi$ ). Additionally, the leg length ranges  $[\rho_i^{\min}, \rho_i^{\max}]$  which lead to the maximal singularity-free orientation workspace can be also determined. The advantage of the Roll–Pitch–Yaw angles is that all rotations  $\mathbf{R}(x, \phi)$ ,  $\mathbf{R}(y, \theta)$  and  $\mathbf{R}(z, \psi)$  take place with respect to the fixed frame. Hence, the obtained orientation is given as

$$\mathbf{Q} = \mathbf{R}(z, \psi)\mathbf{R}(y, \theta)\mathbf{R}(x, \phi). \quad (1)$$

So far, the Roll–Pitch–Yaw angles are widely used in aviation, image navigation, computer vision as well as robotics. They have already become a standard convention in practice. Hence, when an engineer reads Eq. (1), he/she always realizes that the orientation is obtained by the following process: the platform rotates by an angle  $\phi$  around the  $x$ -axis of the fixed frame; then rotates by an angle  $\theta$  around the  $y$ -axis of the fixed frame and finally rotates by an angle  $\psi$  around the  $z$ -axis of the fixed frame. If the orientation workspace in the 3D orientation Cartesian space  $O\phi\theta\psi$  is determined, any point inside the workspace provides a clear measure for the platform to, respectively, rotate in order around the  $(x, y, z)$  axes of the fixed frame.

## 2. Workspace surface

Although the algorithm presented in this work does not lose generality and can be applied to any type of Gough–Stewart platforms, the MSSM (Minimal Simplified Symmetric Manipulator) is chosen for demonstration. The reason is that the Gough–Stewart platforms used in practice are usually very close to the MSSM architecture for stability and simplicity.

As shown in Fig. 1, the MSSM consists of a mobile platform  $P_1(P_6)P_2(P_3)P_4(P_5)$  and a base  $B_1(B_2)B_3(B_4)B_5(B_6)$  connected via six identical UPS legs ( $B_iP_i$ ,  $i = 1, 2, \dots, 6$ ). Both the platform and the base are symmetric.

Considering the symmetry, the fixed frame  $Oxyz$  is attached to the base by selecting  $B_1(B_2)$  as the origin  $O$  and making the  $y$ -axis coincide with the line of symmetry. Besides, the  $Oxy$  plane coincides with the base triangle. Hence, the positions of  $B_i$  ( $i = 1, 2, \dots, 6$ ) in the fixed frame are, respectively,  $\mathbf{b}_1 = \mathbf{b}_2 = [0, 0, 0]^T$ ,  $\mathbf{b}_3 = \mathbf{b}_4 = [t_1, t_2, 0]^T$  and  $\mathbf{b}_5 = \mathbf{b}_6 = [-t_1, t_2, 0]^T$ . Only two geometric parameters are used to describe the base. Similarly, the mobile frame  $O'x'y'z'$  is attached to the platform by selecting the midpoint of line segment  $P_1P_2$  as the origin  $O'$  and  $P_1P_2$  as the  $x'$ -axis. Besides, the  $O'x'y'$  plane coincides with the platform

仅用两个量  $t_1, t_2$  表示  $B_i$       只用  $t_1$  表示  $P_i$

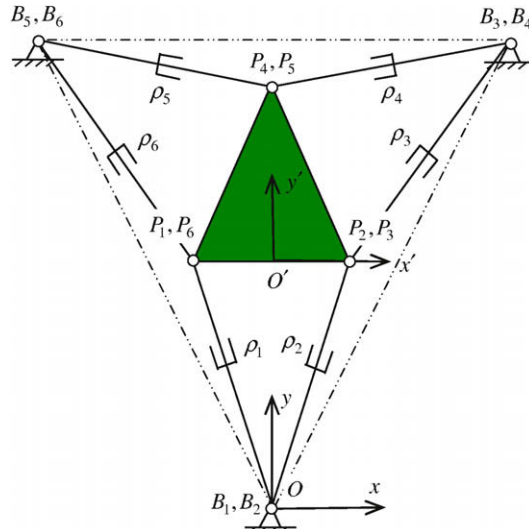


**Fig. 1.** The MSSM architecture (top view).

triangle. The positions of  $P_i$  ( $i = 1, 2, \dots, 6$ ) in the mobile frame are, respectively,  $\mathbf{p}'_1 = \mathbf{p}'_6 = [-t_3, 0, 0]^T$ ,  $\mathbf{p}'_2 = \mathbf{p}'_3 = [t_3, 0, 0]^T$  and  $\mathbf{p}'_4 = \mathbf{p}'_5 = [0, t_4, 0]^T$ . Also, only two geometric parameters are used to describe the platform. Hence, the total number of geometric parameters is only 4.

Let  $\mathbf{Q}$  denote the rotation matrix representing the rotation of the platform from the fixed frame  $Oxyz$  to the mobile frame  $O'x'y'z'$ . From Eq. (1), one obtains

$$\mathbf{Q} = \begin{bmatrix} c\theta c\psi & s\phi s\theta c\psi - c\phi s\psi & c\phi s\theta c\psi + s\phi s\psi \\ c\theta s\psi & s\phi s\theta s\psi + c\phi c\psi & c\phi s\theta s\psi - s\phi c\psi \\ -s\theta & s\phi c\theta & c\phi c\theta \end{bmatrix}, \quad (2)$$

where  $c\phi = \cos\phi$ ,  $s\phi = \sin\phi$ , etc.

$P$  和  $P'$  是末端执行器(运动平台)一点相对固定和移动点的位向量

Let vector  $\mathbf{p}_r = [x_r, y_r, z_r]^T$  denote the position of the origin  $O'$  of the mobile frame in the fixed frame. The position vector of the end-effector  $P$  of the platform in the fixed and mobile frames is, respectively,  $\mathbf{p} = [x, y, z]^T$  and  $\mathbf{p}' = [x_p, y_p, z_p]^T$ . One then has

$$\mathbf{p} = \mathbf{p}_r + \mathbf{Q}\mathbf{p}' \quad (3)$$

or

$$\mathbf{Q} \cdot \text{为什么还有 } \mathbf{p}_r = \mathbf{P} - \mathbf{Q}\mathbf{p}'$$

$$\mathbf{p}_r = \mathbf{p} - \mathbf{Q}\mathbf{p}' \quad (4)$$

Hence, the position of  $P_i$  ( $i = 1, 2, \dots, 6$ ) in the fixed frame can be expressed as

$$\mathbf{p}_i = \mathbf{p}_r + \mathbf{Q}\mathbf{p}'_i = \mathbf{p} + \mathbf{Q}(\mathbf{p}'_i - \mathbf{p}'). \quad \vec{\alpha} \cdot \vec{\beta} = |\vec{\alpha}| |\vec{\beta}| \cos\theta \quad \vec{\alpha} \cdot \vec{\alpha} = |\vec{\alpha}|^2 = \vec{\alpha}^T \vec{\alpha} \quad (5)$$

The length  $\rho_i$  of leg  $i$  is the distance between points  $B_i$  and  $P_i$ . From this, one obtains

$$\rho_i^2 = (\mathbf{p}_i - \mathbf{b}_i)^T (\mathbf{p}_i - \mathbf{b}_i) = [\mathbf{p} + \mathbf{Q}(\mathbf{p}'_i - \mathbf{p}') - \mathbf{b}_i]^T [\mathbf{p} + \mathbf{Q}(\mathbf{p}'_i - \mathbf{p}') - \mathbf{b}_i]. \quad \text{平台质心 } C \text{ 作为平台上任一点。} \quad (6)$$

If the centroid  $C_p$  of the platform is taken as the end-effector  $P$ , then the position of  $P$  in the mobile frame is  $\mathbf{p}' = [0, t_4/3, 0]^T$ . By substituting  $\mathbf{p}$ ,  $\mathbf{p}'$ ,  $\mathbf{p}'_i$  and  $\mathbf{b}_i$  into Eq. (6), the following equation can be obtained for six legs:

$$\left\{ \begin{array}{l} \rho_1^2 = \left[ \frac{2}{3}t_4(xc\phi - ys\phi s\theta) - 2t_3yc\theta \right]s\psi - [2t_3xc\theta + \frac{2}{3}t_4(xs\phi s\theta + yc\phi)]c\psi + 2t_3zs\theta \\ \quad - \frac{2}{3}t_4zs\phi c\theta + t_3^2 + \frac{1}{9}t_4^2 + x^2 + y^2 + z^2, \\ \rho_2^2 = \left[ \frac{2}{3}t_4(xc\phi - ys\phi s\theta) + 2t_3yc\theta \right]s\psi + [2t_3xc\theta - \frac{2}{3}t_4(xs\phi s\theta + yc\phi)]c\psi - 2t_3zs\theta \\ \quad - \frac{2}{3}t_4zs\phi c\theta + t_3^2 + \frac{1}{9}t_4^2 + x^2 + y^2 + z^2, \\ \rho_3^2 = \left[ \frac{2}{3}t_4c\phi(x - t_1) + (\frac{2}{3}t_4s\phi s\theta - 2t_3c\theta)(t_2 - y) \right]s\psi + [(\frac{2}{3}t_4s\phi s\theta - 2t_3c\theta)(t_1 - x) + \frac{2}{3}t_4c\phi(t_2 - y)]c\psi \\ \quad - 2t_3zs\theta - \frac{2}{3}t_4zs\phi c\theta + t_1^2 + t_2^2 + t_3^2 + \frac{1}{9}t_4^2 - 2t_1x - 2t_2y + x^2 + y^2 + z^2, \\ \rho_4^2 = \frac{4}{3}t_4[s\phi s\theta(y - t_2) + c\phi(t_1 - x)]s\psi + \frac{4}{3}t_4[s\phi s\theta(x - t_1) + c\phi(y - t_2)]c\psi \\ \quad + \frac{4}{3}t_4zs\phi c\theta + t_1^2 + t_2^2 + \frac{4}{9}t_4^2 - 2t_1x - 2t_2y + x^2 + y^2 + z^2, \\ \rho_5^2 = \frac{4}{3}t_4[s\phi s\theta(y - t_2) - c\phi(t_1 + x)]s\psi + \frac{4}{3}t_4[s\phi s\theta(x - t_1) + c\phi(y - t_2)]c\psi \\ \quad + \frac{4}{3}t_4zs\phi c\theta + t_1^2 + t_2^2 + \frac{4}{9}t_4^2 + 2t_1x - 2t_2y + x^2 + y^2 + z^2, \\ \rho_6^2 = \left[ \frac{2}{3}t_4c\phi(x + t_1) + (\frac{2}{3}t_4s\phi s\theta + 2t_3c\theta)(t_2 - y) \right]s\psi - [(\frac{2}{3}t_4s\phi s\theta - 2t_3c\theta)(t_1 + x) \\ \quad - \frac{2}{3}t_4c\phi(t_2 - y)]c\psi + 2t_3zs\theta - \frac{2}{3}t_4zs\phi c\theta + t_1^2 + t_2^2 + t_3^2 + \frac{1}{9}t_4^2 + 2t_1x - 2t_2y + x^2 + y^2 + z^2. \end{array} \right. \quad 6 \text{ 个约束环(运动链)方程} \quad (7)$$

For a given architecture, the geometric parameters ( $t_1, t_2, t_3, t_4$ ) are constants. When the position of the end-effector  $P$  is given by  $P_0$ , its three coordinates ( $x, y, z$ ) will also become three constants ( $x_0, y_0, z_0$ ). If  $\phi$ ,  $\theta$  and  $\psi$  remain variable, the leg length will be a function of only  $\phi$ ,  $\theta$  and  $\psi$ . In this case, the above equation can be rewritten as follows:

$$\rho_i = \rho_i(\phi, \theta, \psi) \quad (i = 1, 2, \dots, 6). \quad \text{轨迹几何参数化, } t_1, t_2, t_3, t_4 \text{ 移动坐标系位向量是 } (x_0, y_0, z_0) \quad (8)$$

For a given leg length, Eq. (8) describes a surface in the 3D orientation Cartesian space  $O\phi\theta\psi$ . For six legs, if the leg length ranges are given, there may be up to 12 surfaces: six correspond to the maximal leg lengths and six correspond to the minimal leg lengths. These 12 surfaces can be referred to as the orientation workspace surfaces or simply workspace surfaces because patches of them can become the boundary of the orientation workspace, as shown in Fig. 2.

6个约束环 6个约束方程 = 12个曲面 — 12个工作空间

### 3. Singularity locus

Differentiating Eq. (6) with respect to time, one obtains

$$\rho_i \dot{\rho}_i = (\mathbf{p}_i - \mathbf{b}_i)^T \dot{\mathbf{p}} + [\mathbf{Q}(\mathbf{p}'_i - \mathbf{p}') \times (\mathbf{p}_i - \mathbf{b}_i)]^T \boldsymbol{\omega}, \quad ? \quad (9)$$

where  $\boldsymbol{\omega}$  is the angular velocity of the platform. For all six legs, Eq. (9) can be rewritten as follows:

$$\mathbf{A}\mathbf{v} = \mathbf{D}\dot{\rho}, \quad (10)$$

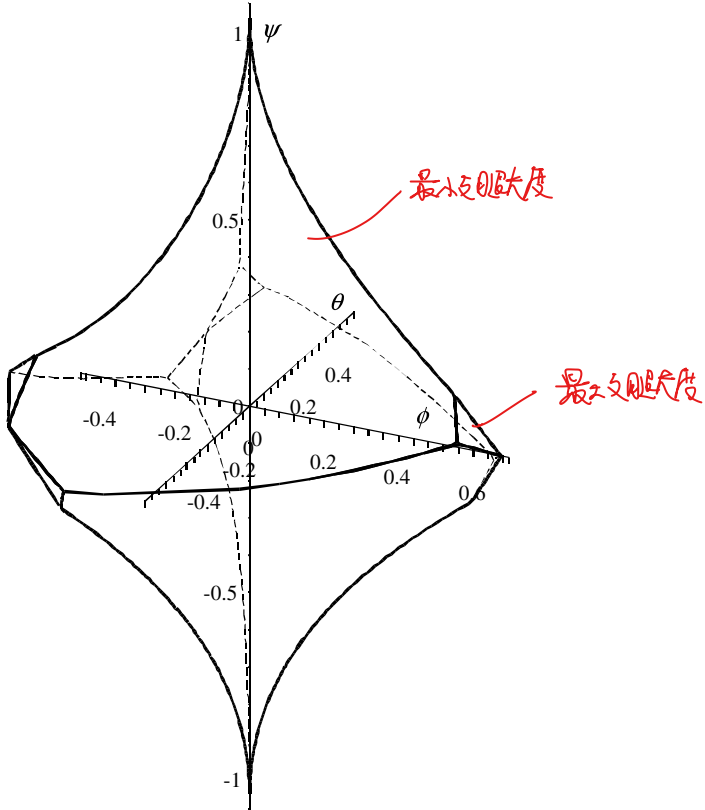


Fig. 2. The orientation workspace at  $P_0(0, \frac{2\sqrt{3}}{3}, \frac{5}{4})$  with  $\rho_i^{\max} = 1.75$  and  $\rho_i^{\min} = 1.30$ .

where  $\dot{\rho} = [\dot{\rho}_1, \dot{\rho}_2, \dots, \dot{\rho}_6]^T$  denotes the actuator velocities and  $\mathbf{v} = [\mathbf{p}^T, \omega^T]^T$  the Cartesian velocity vector of the platform.  $\mathbf{A}$  and  $\mathbf{D}$  are two Jacobian matrices.  $\mathbf{D} = \text{diag}(\rho_1, \rho_2, \dots, \rho_6)$ .

The singularity condition is  $\det(\mathbf{A}) = 0$ . As shown in [8], the determinant of matrix  $\mathbf{A}$  can be expanded using linear decomposition. Hence, the obtained singularity equation can be given as follows:

~~矩阵行列式线性展开~~

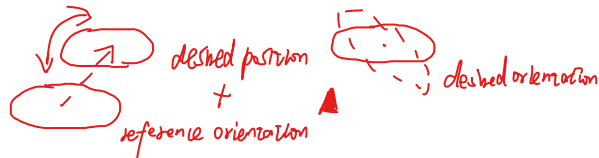
$$f_1x^2z + f_2x^2 + f_3xyz + f_4xy + f_5xz^2 + f_6xz + f_7x + f_8y^2z + f_9y^2 + f_{10}yz^2 + f_{11}yz + f_{12}y + f_{13}z^3 + f_{14}z^2 + f_{15}z + f_{16} = 0, \quad (11)$$

where  $f_i = f_i(\phi, \theta, \psi)$  ( $i = 1, 2, \dots, 16$ ).

At a given position  $P_0(x_0, y_0, z_0)$ , the singularity locus given by Eq. (11) in the 3D orientation Cartesian space  $O\phi\theta\psi$  is a surface as shown in Fig. 3.

#### 4. Maximal singularity-free orientation workspace

##### 4.1. Definition



As mentioned in Section 2, the orientation workspace can be defined by up to 12 workspace surfaces that depend on the maximal and minimal leg lengths of each leg. Hence, the total number of variables is 12. In Fig. 2, the base is an equilateral triangle of unit area. Suppose the size ratio between the platform and the base is  $\frac{3}{5}$ . Hence, the geometric parameters can be given as  $t_1 = \frac{1}{\sqrt{3}}$ ,  $t_2 = \sqrt[4]{3}$ ,  $t_3 = \frac{3}{5\sqrt{3}}$  and  $t_4 = \frac{3\sqrt[4]{3}}{5}$ . The centroid of the platform is taken as the considered point  $P$ . The position of the platform is prescribed at  $P_0(0, \frac{2\sqrt{3}}{3}, \frac{5}{4})$ . The maximal and minimal leg lengths are chosen as  $\rho_i^{\max} = 1.75$  and  $\rho_i^{\min} = 1.30$ .

Considering that the Roll-Pitch-Yaw angles are used to define an orientation and the MSSM is symmetric, the platform has the same chance to rotate around the  $x$ -,  $y$ -,  $z$ -axes of the fixed frame in the clockwise or anticlockwise directions. Furthermore, in practice, the platform usually translates to the desired position in the reference orientation  $(0, 0, 0)$  first and then rotates to the desired orientation. Therefore, it is reasonable to take the leg lengths in the reference orientation  $(0, 0, 0)$  as the nominal leg lengths. In the considered case, the nominal leg length is  $\rho_i^{\text{nom}} = 1.465452$  ( $i = 1, 2, \dots, 6$ ). It is easy to find that the minimal leg length  $\rho_i^{\min}$  is closer to the nominal leg length  $\rho_i^{\text{nom}}$  than the maximal leg length  $\rho_i^{\max}$ . In Fig. 2, the minimal leg lengths correspond to the six large patches of workspace boundary and the maximal leg lengths correspond to the six small patches of workspace boundary. To balance these 12 patches of workspace boundary, one idea is to make the difference between the minimal leg length and the nominal leg length be equal to that between the maximal leg length and the nominal leg length, i.e.,

~~为平衡曲面大小，平衡腿长最好在最大最小腿长中值附近~~

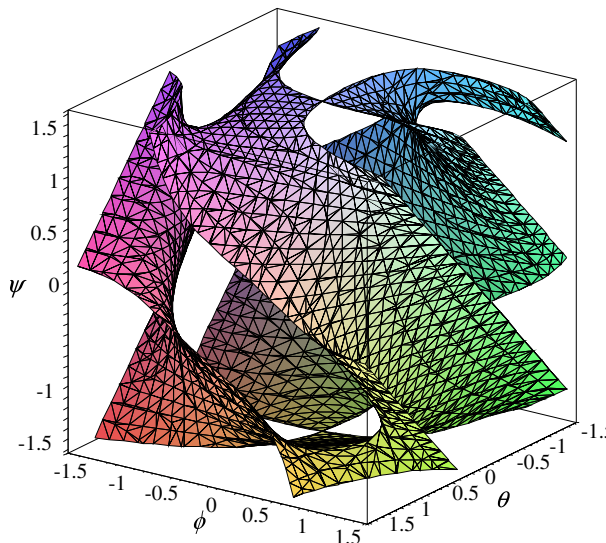


Fig. 3. Singularity locus at a given position  $P_0(0, \frac{2\sqrt{3}}{3}, \frac{5}{4})$ .

$$D = |\rho_i^{\min} - \rho_i^{\text{nom}}| = |\rho_i^{\max} - \rho_i^{\text{nom}}| \quad (i = 1, 2, \dots, 6). \quad Q: \text{为什么定位工作空间反而随} D \text{确定?} \quad (12)$$

As a result, the orientation workspace is determined by only one variable  $D$ , which is referred to as the orientation workspace variable. If  $D$  changes, the shape and the size of the orientation workspace changes accordingly. When  $D$  takes its limit value  $D_{\lim}$ , the boundary of the orientation workspace just touches the singularity surface at some point(s). In this status, the singularity-free orientation workspace becomes the maximum. In other words, the maximal singularity-free orientation workspace is determined by  $D_{\lim}$ . 变号大误差

However, it is very difficult to determine  $D_{\lim}$  analytically because the shape of the orientation workspace is very complex. Hence, a numerical algorithm is presented to solve this problem. The basic idea is to increase  $D$  from 0 until the boundary of the orientation workspace just touches the singularity surface at some point(s). The general procedure can be described as follows: First, set the orientation workspace variable  $D$  to 0. Then, increase  $D$  by one step  $\Delta D$  and verify whether any singularity exists inside the obtained orientation workspace. If no singularity exists, continue to increase  $D$  with the same step size  $\Delta D$ . Otherwise, the used step size is too large for this step. In this case, restore  $D$  to its previous value and reduce the step size  $\Delta D$  by one half. Then, increase  $D$  by the reduced step size  $\Delta D$ . Repeat this procedure until  $D$  converges at its limit value  $D_{\lim}$ . At this moment, the step size  $\Delta D$  becomes very small and the singularity-free workspace reaches the maximum. In order to make the procedure more efficient, the initial value of the step size  $\Delta D$  is not necessarily very small. The detailed procedure will be given later.

#### 4.2. Workspace volume

For a given reasonable value of the orientation workspace variable  $D$ , there exists an orientation workspace in the 3D orientation Cartesian space  $O\phi\theta\psi$ . Although the volume of such a 3D orientation workspace is not straightforward and easy to understand [23], it can be used as the measure of the orientation workspace.

To guarantee no singularity inside the obtained orientation workspace, it is necessary to perform singularity verification. However, in the 3D orientation Cartesian space  $O\phi\theta\psi$ , both the orientation workspace and the singularity surface are very complex. To directly determine whether any singularity exists inside the 3D orientation workspace is not convenient. Comparatively, the singularity verification in a 2D workspace section at a given  $\theta$  is easy. Moreover, if every workspace section is singularity-free, the entire workspace should be singularity-free.

However, there are infinitely many workspace sections and hence it is impossible to verify every one. One solution to this problem is to verify only a few workspace sections which are used to evaluate the workspace volume. The density of these workspace sections depends on the convergence precision. In other words, when the workspace volume converges at a given precision, two neighbouring workspace sections can be regarded as sufficiently close. For a given  $D$ , the workspace volume  $V$  can be given by the following equation:

$$V \approx \sum_{i=1}^n \frac{(A_{i-1} + A_i)\Delta\theta}{2}, \quad \text{公式计算本积, 且元面积小, 体积越精确} \quad (13)$$

where  $A_i$  ( $i = 0, 1, \dots, n$ ) is the area of the workspace section at  $\theta_i$ .

假设各关节是在直角坐标系内

Unfortunately, the number  $n$  is hard to determine because the maximal and minimal  $\theta$  coordinates of the orientation workspace are unknown. Assuming that the reference orientation  $(0, 0, 0)$  always exists inside the orientation workspace, a valid workspace section should exist in the plane with  $\theta = 0$  even if it shrinks to one point in some special cases. Hence, the orientation workspace can be divided into two parts: one with  $\theta \leq 0$  and the other with  $\theta \geq 0$ . Take the part with  $\theta \leq 0$  as an example, its volume  $V_1$  can be given as

$$V_1 \approx \sum_{i=1}^{n_1} \frac{(A_{i-1} + A_i)\Delta\theta}{2}, \quad (14)$$

where  $A_0$  is the area of the workspace section with  $\theta = 0$ . The number  $n_1$  can be determined as follows: for a given step size  $\Delta\theta$ ,  $n_1$  is the maximal number of the steps for  $\theta$  to decrease from 0 until a value  $(-n_1\Delta\theta)$  at which the corresponding workspace section vanishes, i.e.,  $A_{n_1} = 0$ .

The volume  $V_2$  of the other part of the workspace with  $\theta \geq 0$  can be computed in a similar way. When  $V_1$  and  $V_2$  are available, their sum is the volume  $V$  of the entire workspace.

Hence, the computation of the workspace volume is twofold: when  $D$  has not reached its limit value  $D_{\lim}$ , the objective is just to perform singularity verification. When  $D$  reaches its limit value  $D_{\lim}$ , the volume of the maximal singularity-free orientation workspace is obtained. Obviously, if  $D$  exceeds its limit value  $D_{\lim}$ , the workspace intersects the singularity surface. In this case, the computation of the workspace volume cannot continue. Instead, restore  $D$  to its previous value and reduce the step size  $\Delta D$  by one half. Then, use the new step size  $\Delta D$  to increase  $D$  in order to obtain a new singularity-free orientation workspace.

For programming convenience,  $A_{i-1}$  and  $A_i$  in Eqs. (13) and (14) are, respectively, denoted by  $A_0$  and  $A$ , see Fig. 5.

#### 4.3. Workspace section

To compute the volume of the orientation workspace as well as to verify whether any singularity exists inside the workspace, it is necessary to define the workspace section. For a given valid  $\theta_i$  which is inside the orientation workspace, there should exist a workspace section in the plane with  $\theta = \theta_i$  – which is parallel to the  $O\phi\psi$  plane – as shown in Fig. 4. For any point inside the workspace section, if its coordinates  $(\phi, \theta_i, \psi)$  are substituted into Eq. (8), the obtained leg length should satisfy the following condition:

$$\rho_i^{\min} \leq \rho_i \leq \rho_i^{\max} \quad (i = 1, 2, \dots, 6). \quad \text{只考虑单侧约束} \quad (15)$$

The area  $A_i$  of the workspace section with  $\theta = \theta_i$  can be given as

$$A_i \approx \sum_{j=1}^m \frac{(h_{j-1}^\psi + h_j^\psi)\Delta\phi}{2}, \quad \text{给定}\theta = \theta_i, \theta_{i-1} \text{时单侧上下表面积 } A_{i-1} \text{ 和 } A_i \quad (16)$$

where  $h_j^\psi$  ( $j = 0, 1, \dots, m$ ) is the height of the workspace section in the  $\psi$ -direction at  $\phi_j$ , see Fig. 4.

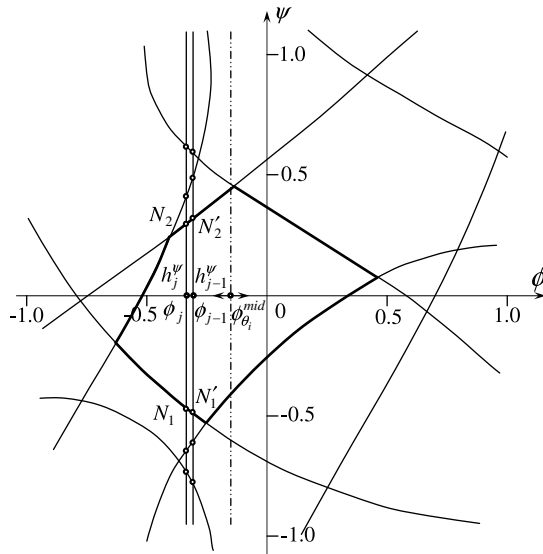


Fig. 4. The workspace section in the plane:  $\theta = \theta_i$ .

However, the number  $m$  is also hard to determine because the maximal and minimal  $\phi$  coordinates of the workspace section are unknown. Considering that two neighbouring workspace sections are very close, the workspace section can be divided into two parts by  $\phi_{\theta_i}^{\text{mid}}$ : one with  $\phi \leq \phi_{\theta_i}^{\text{mid}}$  and the other with  $\phi \geq \phi_{\theta_i}^{\text{mid}}$ . Here,  $\phi_{\theta_i}^{\text{mid}}$  is the average value of the maximal and minimal valid  $\phi$  values of the previous workspace section, i.e.,  $\phi_{\theta_i}^{\text{mid}} = (\phi_{\theta_{i-1}}^{\text{max}} + \phi_{\theta_{i-1}}^{\text{min}})/2$ . When  $\theta = 0$ ,  $\phi_0^{\text{mid}}$  takes 0 which is the  $\phi$  coordinate of the reference orientation (0, 0, 0). Take the part with  $\phi \leq \phi_{\theta_i}^{\text{mid}}$  as an example, its area  $A_{i1}$  can be given as

$$A_{i1} \approx \sum_{j=1}^{m_1} \frac{(h_{j-1}^\psi + h_j^\psi)\Delta\phi}{2}, \quad (17)$$

当  $h_{m_1}^\psi < 0$  时，我们认为找到了  $\phi_{\theta_i}^{\text{mid}}$  或  $\phi_{\theta_i}^{\text{min}}$  所在的位置，但是是  $\phi = \phi_{\theta_i}^{\text{mid}}$  时的高度

where  $h_j^\psi$  is the height of the workspace section at  $\phi = \phi_{\theta_i}^{\text{mid}}$ . The number  $m_1$  can be determined as follows: for a given step size  $\Delta\phi$ ,  $m_1$  is the maximal number of the steps for  $\phi$  to decrease from  $\phi_{\theta_i}^{\text{mid}}$  until a value ( $\phi_{\theta_i}^{\text{mid}} - m_1\Delta\phi$ ) at which the corresponding workspace height vanishes, i.e.,  $h_{m_1}^\psi = 0$ .

The area  $A_{i2}$  of the other part with  $\phi \geq \phi_{\theta_i}^{\text{mid}}$  can be computed in a similar way. When  $A_{i1}$  and  $A_{i2}$  are available, their sum is the area  $A_i$  of the entire workspace section with  $\theta = \theta_i$ .

For programming convenience,  $A_{i1}$  and  $A_{i2}$  are, respectively, denoted by  $A_1$  and  $A_2$ ;  $h_{j-1}^\psi$  and  $h_j^\psi$  are, respectively, denoted by  $h_0^\psi$  and  $h^\psi$ , see Fig. 5.

#### 4.4. Computation of $h^\psi$

To compute the area of the workspace section with  $\theta = \theta_i$ , it is necessary to compute the height  $h_j^\psi$  of the workspace section in the  $\psi$ -direction at a given  $\phi_j$ , see Fig. 4. In the plane with  $\theta = \theta_i$ , every workspace surface given by Eq. (8) becomes a curve, which can be referred to as the workspace curve. For given leg length ranges, the total number of the workspace curves is 12: six correspond to the maximal leg lengths and the other six correspond to the minimal leg lengths. Fig. 4 shows that there are only eight workspace curves close to the considered workspace section in this case. The other four workspace curves do not appear in the region as shown in this figure.

To compute the possible intersections of each workspace curve and the line  $\phi = \phi_j$  in the workspace section plane, just substitute  $\phi$  by  $\phi_j$  into Eq. (7), a single variable equation in  $\psi$  can be obtained as follows:

$$a_i \sin \psi + b_i \cos \psi + c_i = 0 \quad (i = 1, 2, \dots, 12). \quad (18)$$

From Eq. (18)

$$\psi = 2 \tan^{-1} \left( \frac{-a_i \pm \sqrt{\Delta}}{c_i - b_i} \right) \quad (i = 1, 2, \dots, 12), \quad (19)$$

④：求出交点后还要对交点圆弧取整除法

where  $\Delta = a_i^2 + b_i^2 - c_i^2$ . If  $\Delta > 0$ , Eq. (19) gives two real solutions for Eq. (18) in the range  $[-\pi, \pi]$ ; if  $\Delta = 0$ , Eq. (19) gives only one real solution in the range  $[-\pi, \pi]$ ; and if  $\Delta < 0$ , there is no real solution for Eq. (18). In other words, if  $\Delta > 0$ , there are two intersections of the considered workspace curve and the line  $\phi = \phi_j$ ; if  $\Delta = 0$ , there is only one intersection; and if  $\Delta < 0$ , there is no intersection.

When all intersections are available, then select those lying on the boundary of the workspace section using the condition of Eq. (15). Then, order these intersections using their  $\psi$  coordinates. For two neighbouring intersections, say  $N_1$  and  $N_2$  in Fig. 4, if any point on  $\overline{N_1 N_2}$  also satisfies Eq. (15),  $\overline{N_1 N_2}$  is a contribution of  $h_j^\psi$ . Summing up all contributions,  $h_j^\psi$  can be obtained. In general, there is only one such segment for  $h_j^\psi$ , see Fig. 4.

#### 4.5. Singularity verification

$N, N' N_1 N_2' \rightarrow$  代入奇异轨迹得细的  $F, F' F_1 F_2'$  中向右移  $F, F' \rightarrow$   $F_2 F_1'$  右侧证明不穿过奇异性

The singularity verification is performed in each workspace section. Referring to Fig. 4, if every small quadrilateral ( $N_1 N_2 N'_2 N'_1$ ) between  $\phi_j$  and  $\phi_{j-1}$  is singularity-free, the entire workspace section is singularity-free. To verify whether any singularity exists inside this small quadrilateral, substitute the coordinates of the four vertices ( $N_1, N_2, N'_2, N'_1$ ) into the singularity expression (the left-hand side of Eq. (11)), there are four function values ( $F_1, F_2, F'_2, F'_1$ ). If all these function values take the same sign, there is no side of the small quadrilateral ( $N_1 N_2 N'_2 N'_1$ ) intersecting the singularity curve. The reason is: when the area of the workspace section converges, the step size  $\Delta\phi = |\phi_j - \phi_{j-1}|$  becomes very small. If  $F_1 F'_1 > 0$ , there is no intersection between the boundary arc  $N_1 N'_1$  of the workspace section and the singularity curve. Similarly, if  $F_2 F'_2 > 0$ , there is no intersection between the boundary arc  $N_2 N'_2$  of the workspace section and the singularity curve. And if there is no intersection between the boundary of workspace section and the singularity curve, it is impossible for any line segment (say  $N_1 N_2$  or  $N'_1 N'_2$ ) inside the workspace section to intersect the singularity curve. Hence, the function values ( $F_1, F_2, F'_2, F'_1$ ) should take the same sign. If not, the small quadrilateral ( $N_1, N_2, N'_2, N'_1$ ) will contain part of the singularity curve.

#### 4.6. Computation procedure

The procedure for determining the maximal singularity-free orientation workspace is shown in Fig. 5. Details are illustrated as follows:

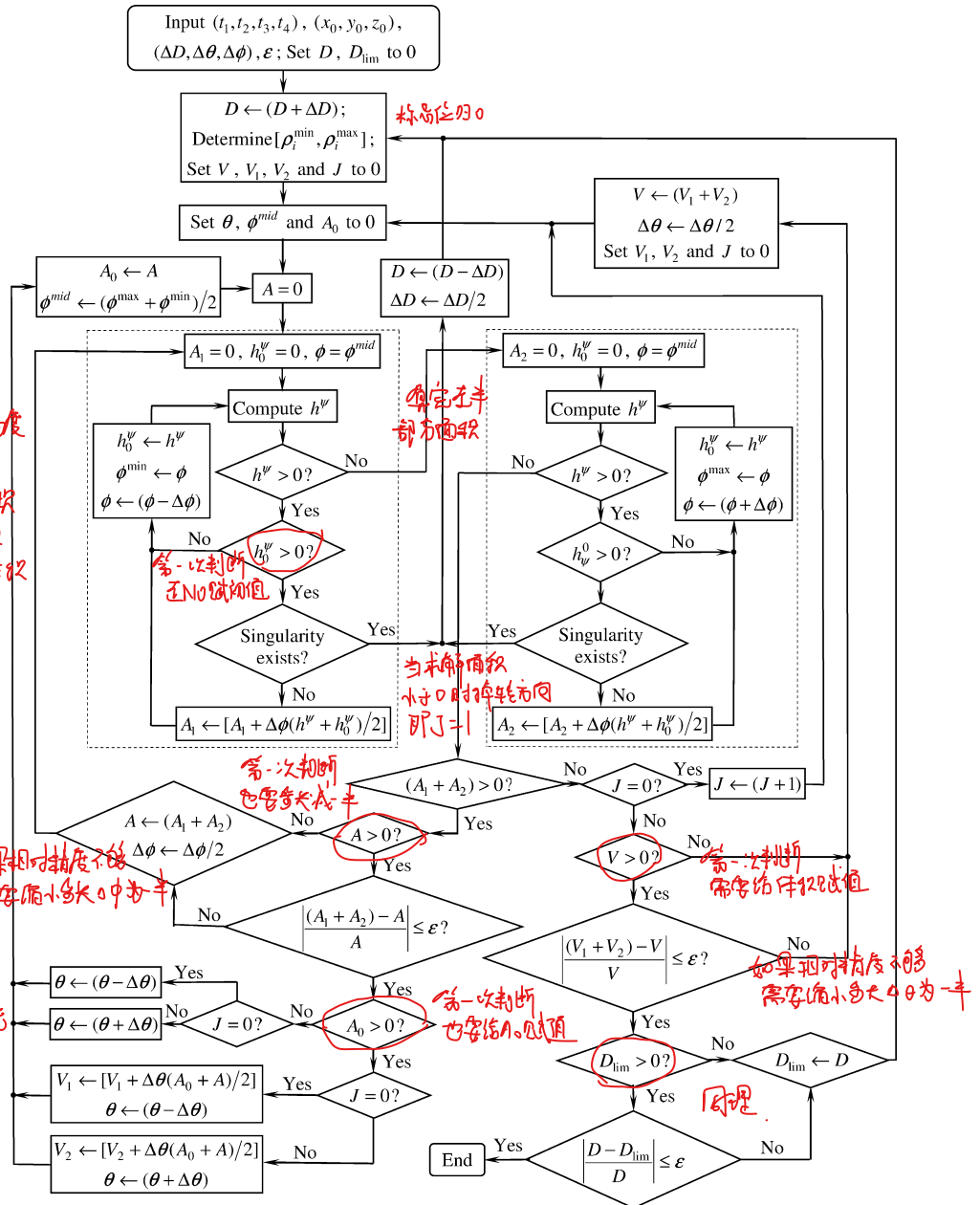


**Fig. 5.** Procedure for determining the maximal singularity-free orientation workspace.

- **Step 1:** Input the geometric parameters  $(t_1, t_2, t_3, t_4)$ , the coordinates  $(x_0, y_0, z_0)$  of the prescribed position  $P_0$  of the platform, the initial step sizes  $(\Delta D, \Delta \theta, \Delta \phi)$  as well as the convergence precision  $\varepsilon$ . Set  $D$  and  $D_{\text{lim}}$  to 0.
  - **Step 2:** Increase  $D$  by  $\Delta D$  and compute the leg length ranges  $[\rho_i^{\min}, \rho_i^{\max}]$  ( $i = 1, 2, \dots, 6$ ). Set  $V, V_1, V_2$  and  $J$  to 0. If  $J = 0$ , compute the volume  $V_1$  of the orientation workspace with  $\theta \leq 0$ . Else if  $J = 1$ , compute the volume  $V_2$  of the orientation workspace with  $\theta \geq 0$ .
  - **Step 3:** Set  $\theta, \phi^{\text{mid}}$  and  $A_0$  to 0. This means that the computation starts from the workspace section with  $\theta = 0$ .
  - **Step 4:** Set  $A$  to 0.
  - **Step 5:** Compute the area  $A_1$  of the workspace section with  $\phi \leq \phi^{\text{mid}}$ . The computation procedure for  $A_1$  is given by the left dashed rectangular frame in Fig. 5, which can be described as follows:
    - **Step 5.1:** Set the initial values of  $A_1$  and  $h_0^\psi$  to 0. Let  $\phi$  equal to  $\phi^{\text{mid}}$ . This means that the computation starts from  $\phi = \phi^{\text{mid}}$ .
    - **Step 5.2:** Compute  $h^\psi$  using the method described in Section 4.4. If  $h^\psi > 0$ , continue. Otherwise, go to Step 6.

- Step 5.3: If  $h_0^\psi > 0$ , continue. Otherwise, go to Step 5.6.
- Step 5.4: Perform singularity verification using the approach mentioned in Section 4.5. If a singularity exists inside the workspace section, restore the previous value of  $D$  and reduce the step size  $\Delta D$  by one half, then go to Step 2.
- Step 5.5: Increase  $A_1$  by  $\Delta\phi(h^\psi + h_0^\psi)/2$ .
- Step 5.6: Give the value of  $h^\psi$  to  $h_0^\psi$  and the value of  $\phi$  to  $\phi^{\min}$ , which denotes the minimal valid  $\phi$  in the considered workspace section. Then, reduce  $\phi$  by one step  $\Delta\phi$  and go to Step 5.2.
- Step 6: Compute the area  $A_2$  of the workspace section with  $\phi \geq \phi^{\min}$  using a similar procedure which is given by the right dashed rectangular frame in Fig. 5.
- Step 7: If  $(A_1 + A_2) > 0$ , continue. Otherwise, go to Step 15.
- Step 8: If  $A > 0$  (the area of the workspace section computed with a larger step size  $\Delta\phi$ ), continue. Otherwise, go to Step 10.
- Step 9: Check the convergence condition. If  $A$  has already reached the desired precision, go to Step 11.
- Step 10: Put the sum of  $A_1$  and  $A_2$  to  $A$ , reduce the step size  $\Delta\phi$  by one half in order to improve the precision and go to Step 5.1.
- Step 11: If  $A_0 > 0$ , continue. Otherwise, go to Step 13.
- Step 12: If  $J = 0$ , increase  $V_1$  by  $\Delta\theta(A + A_0)/2$  and reduce  $\theta$  by one step  $\Delta\theta$ . Else, increase  $V_2$  by  $\Delta\theta(A + A_0)/2$  and  $\theta$  by one step  $\Delta\theta$ . Then, go to Step 14.
- Step 13: If  $J = 0$ , reduce  $\theta$  by one step  $\Delta\theta$ . Else, increase  $\theta$  by one step  $\Delta\theta$ .
- Step 14: Set the value of  $A$  to  $A_0$  and the result of  $(\phi^{\max} + \phi^{\min})/2$  to  $\phi^{\text{mid}}$ . Then, go to Step 4.
- Step 15: If  $J = 0$ , increase  $J$  by 1 and go to Step 3.
- Step 16: If  $V > 0$  (the volume of the orientation workspace computed with a larger step size  $\Delta\theta$ ), continue. Otherwise, go to Step 18.
- Step 17: Check the convergence condition. If  $V$  has already reached the desired precision, go to Step 19.
- Step 18: Put the sum of  $V_1$  and  $V_2$  to  $V$ , reduce the step size  $\Delta\theta$  by one half in order to improve the precision and set  $V_1$ ,  $V_2$  and  $J$  to 0. Then, go to Step 3.
- Step 19: If  $D_{\lim} > 0$ , continue. Otherwise, go to Step 21.
- Step 20: Check the convergence condition. If  $D$  has already reached its limit value  $D_{\lim}$ , output the results and end the computation.
- Step 21: Put the value of  $D$  to  $D_{\lim}$  and go to Step 2.

## 5. Maximal singularity-free sphere

To compare the maximal singularity-free orientation workspace and the maximal singularity-free sphere, an iterative algorithm for determining the maximal singularity-free sphere is presented in this section. The problem consists in finding the point on the singularity surface which is the closest to the reference orientation  $(0,0,0)$ . The formulation can be given as follows:

$$\min_{(\phi,\theta,\psi)} d, \quad (20)$$

where

$$d = \phi^2 + \theta^2 + \psi^2 + \lambda F, \quad (21)$$

where  $\lambda$  is the Lagrange multiplier used to transform the constrained problem into an unconstrained one.  $F$  is the singularity expression, i.e., the left-hand side of Eq. (11). To obtain the extremum of  $d$ , the following condition should be satisfied:

$$\begin{cases} \frac{\partial d}{\partial \phi} = 2\phi + \lambda \frac{\partial F}{\partial \phi} = 0, \\ \frac{\partial d}{\partial \theta} = 2\theta + \lambda \frac{\partial F}{\partial \theta} = 0, \\ \frac{\partial d}{\partial \psi} = 2\psi + \lambda \frac{\partial F}{\partial \psi} = 0, \\ \frac{\partial d}{\partial \lambda} = F = 0. \end{cases} \quad (22)$$

Eliminating  $\lambda$  from Eq. (22), one obtains

$$\theta = \phi \frac{\partial F / \partial \theta}{\partial F / \partial \phi}, \quad (23)$$

$$\psi = \phi \frac{\partial F / \partial \psi}{\partial F / \partial \phi}, \quad (24)$$

$$F = 0. \quad (25)$$

Instead of the resultant method used in [10], an iterative algorithm is used to solve Eqs. (23)–(25). The procedure is as follows: start from a chosen orientation  $(\phi_0, \theta_0, \psi_0)$ . From Eq. (23), a new value  $\theta_1$  can be obtained. And from Eq. (24), a new value  $\psi_1$  can be obtained. Substitute  $\theta_1$  and  $\psi_1$  into Eq. (25), a new value  $\phi_1$  can be obtained in the interval  $[-\pi/2, \pi/2]$

by solving Eq. (25). Then, use the obtained new orientation  $(\phi_1, \theta_1, \psi_1)$  to obtain another new orientation  $(\phi_2, \theta_2, \psi_2)$ . Repeat this procedure until the following convergence condition is satisfied:

$$\sqrt{(\phi_i - \phi_{i-1})^2 + (\theta_i - \theta_{i-1})^2 + (\psi_i - \psi_{i-1})^2} \leq \varepsilon. \quad (26)$$

If the obtained extremum  $d_e$  of  $d$  is the global minimal distance from the reference orientation  $(0, 0, 0)$  to the singularity surface,  $d_e$  will be taken as the radius  $r$  of the maximal singularity-free sphere, i.e.,  $r = d_e$ . However, to be sure that the obtained  $d_e$  is the global minimal distance, singularity verification may be necessary. The singularity verification can be performed in the section with  $\psi = \psi_i$  ( $\psi_i \in [-r, r]$ ) of the sphere with a radius  $r = d_e$ . The number of the used sections is determined by the numerical computation of the volume of the sphere. In other words, when the volume of the sphere computed by the numerical algorithm converges at the volume computed by the analytical formula  $V = \frac{4\pi r^3}{3}$ , two neighbouring sections can be regarded as sufficiently close. The following example will show that the singularity verification is unnecessary.

## 6. Example

To demonstrate the procedure proposed above, consider a MSSM with an equilateral triangle base of unit area. Suppose the platform is also an equilateral triangle and the size ratio between the platform and the base is  $\frac{3}{5}$ . Hence, the geometric parameters are:  $t_1 = \frac{1}{\sqrt[3]{3}}$ ,  $t_2 = \sqrt[4]{3}$ ,  $t_3 = \frac{3}{5\sqrt[3]{3}}$  and  $t_4 = \frac{3\sqrt[4]{3}}{5}$ . Take the centroid  $C_p$  of the platform as the end-effector  $P$ . Its position in the mobile frame  $O'x'y'z'$  is  $\mathbf{p}' = [0, \frac{\sqrt[4]{3}}{5}, 0]^T$ . Suppose the prescribed position of the platform is  $P_0(0, \frac{2\sqrt[4]{3}}{3}, \frac{5}{4})$ , which lies on the perpendicular line through the centroid  $C_b(0, \frac{2\sqrt[4]{3}}{3}, 0)$  of the base. The initial step sizes are chosen as  $\Delta D = 0.1$ ,  $\Delta\theta = \Delta\phi = 0.01$ . The convergence precision is set to  $\varepsilon = 10^{-4}$ .

### 6.1. Computational results

Applying the algorithm presented in Section 4, the determined maximal singularity-free orientation workspace with a volume  $V = 2.967244$  is shown in Fig. 6. The limit value of the orientation workspace variable is  $D_{\lim} = 0.363330$ . As the nominal leg length is  $\rho_i^{\text{nom}} = 1.465452$ , the maximal and the minimal leg lengths are  $\rho_i^{\max} = 1.828782$ ,  $\rho_i^{\min} = 1.102122$  ( $i = 1, 2, \dots, 6$ ). The final step sizes are  $\Delta D = 4.882813 \times 10^{-5}$ ,  $\Delta\theta = \Delta\phi = 0.0025$ .

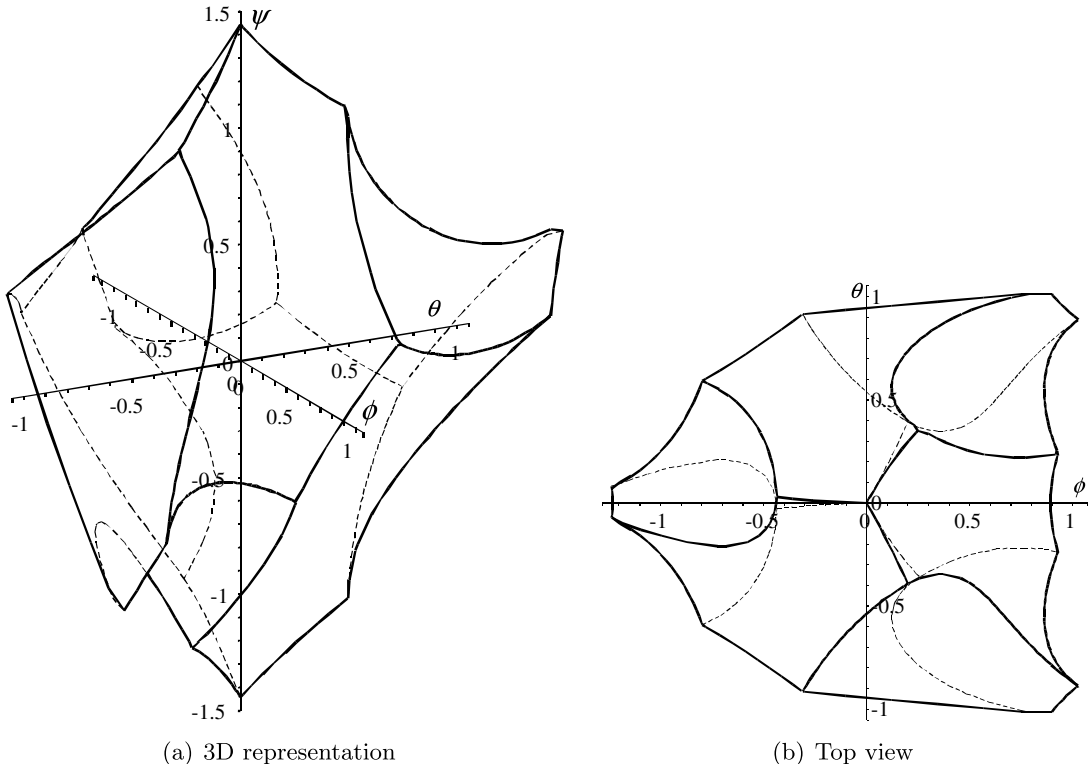


**Fig. 6.** The maximal singularity-free orientation workspace at  $P_0(0, \frac{2\sqrt[4]{3}}{3}, \frac{5}{4})$ .

Applying the iterative algorithm presented in Section 5, the maximal singularity-free sphere centred at the reference orientation  $(0,0,0)$  is determined as shown in Fig. 7. The computation results show that no matter which orientation  $(\phi_0, \theta_0, \psi_0)$  is taken as the starting point, the converged point is always close to  $(-1.233272, 0, 0)$ . For instance, the difference between the converged points from the starting points  $(0,0,0)$  and  $(1,1,1)$  is only  $4.561612 \times 10^{-7}$ . Hence, the distance between point  $(-1.233272, 0, 0)$  and the reference orientation  $(0,0,0)$  should be the global minimal distance. The section circle of the maximal singularity-free sphere in the plane with  $\psi = 0$  is shown in Fig. 8.

To compare the maximal singularity-free orientation workspace and the maximal singularity-free sphere, Fig. 9 shows the situation by putting them together. It can be seen that the maximal singularity-free sphere cannot cover the maximal singularity-free orientation workspace completely, though its volume (7.857153) is 2.649209 times of that (2.967244) of the maximal singularity-free orientation workspace. Fig. 10 shows that both the maximal singularity-free orientation workspace and the maximal singularity-free sphere do not intersect the singularity surface.

## 6.2. Computational cost

The presented algorithm is programmed using Visual C++ 6.0 in a Windows XP environment. The CPU of the used computer is a Pentium IV with 2.4 GHz. The computation for determining the maximal singularity-free sphere is very fast. The computation time at the convergence precision  $\varepsilon = 10^{-6}$  is no more than 1 s.

But the computation time for determining the maximal singularity-free orientation workspace is much longer. If the convergence precision is set to  $\varepsilon = 10^{-4}$ , the computation time is about 165 s. The volume of the maximal singularity-free

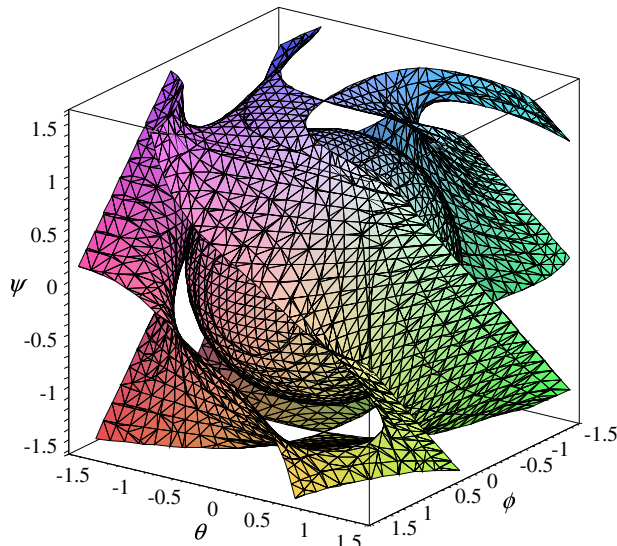


**Fig. 7.** The maximal singularity-free sphere.

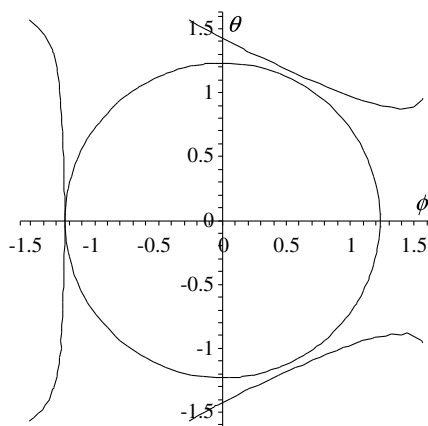


**Fig. 8.** The maximal singularity-free circle on the plane with  $\psi = 0$ .

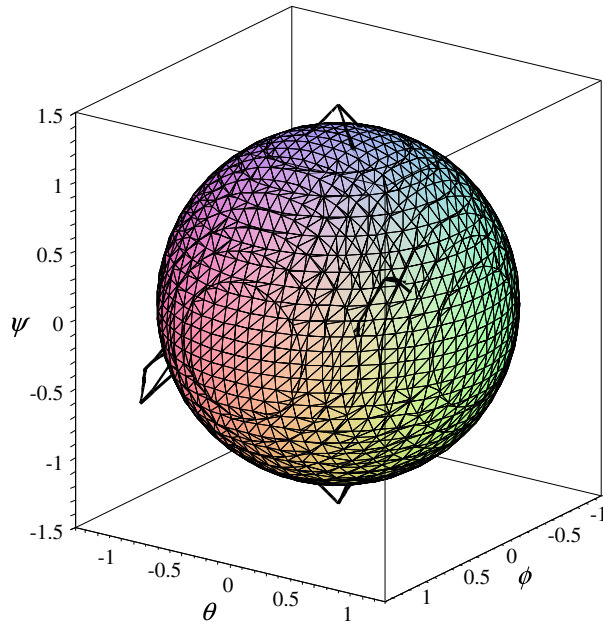


**Fig. 9.** The maximal singularity-free orientation workspace and the maximal singularity-free sphere.

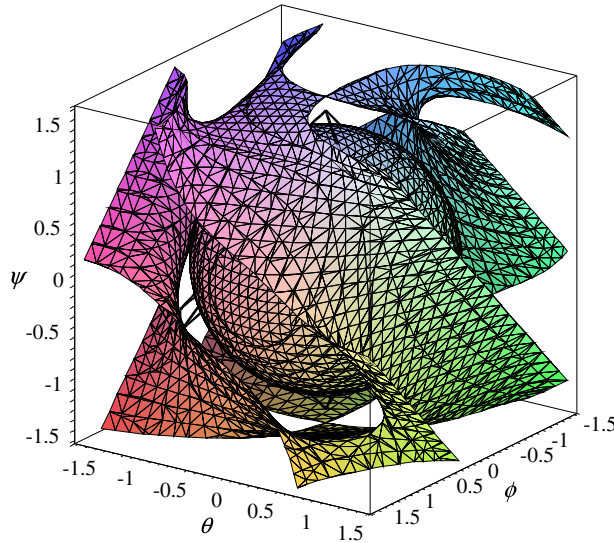


**Fig. 10.** The maximal singularity-free orientation workspace, the maximal singularity-free sphere as well as the singularity surface.

orientation workspace is  $V = 2.965441$  and the final step size  $\Delta D$  is  $4.882813 \times 10^{-5}$ , which is already very small. If the convergence precision is improved to  $\varepsilon = 10^{-5}$ , the computation time is around 345 s. The volume of the maximal singularity-free orientation workspace changes to  $V = 2.965849$  and the final step size  $\Delta D$  changes to  $6.103516 \times 10^{-6}$ . The difference on the computed volume is only 0.000408. Hence,  $\varepsilon = 10^{-4}$  is already a good convergence precision with a reasonable computation time. It is not necessary to increase the convergence precision further.

## 7. Conclusions

To maximize the singularity-free workspace of parallel manipulators is highly desirable in robot design. This work addresses the determination of the 3D maximal singularity-free orientation workspace at a prescribed position of the Gough–Stewart platform. Using the Roll–Pitch–Yaw angles  $(\phi, \theta, \psi)$ , the orientation workspace at a prescribed position can

be defined by up to 12 workspace surfaces. However, it is very difficult to determine these 12 workspace surfaces in order to obtain the maximal singularity-free orientation workspace using an analytical method. Instead, a numerical algorithm is developed to solve this problem. The presented algorithm is able to determine the maximal singularity-free orientation workspace as well as the corresponding leg length ranges  $[\rho_i^{\min}, \rho_i^{\max}]$  ( $i = 1, 2, \dots, 6$ ).

Besides, to compare the maximal singularity-free orientation workspace with the maximal singularity-free sphere, an iterative algorithm for determining the maximal singularity-free sphere is also provided. An example with equilateral triangle base and platform of the MSSM architecture is used to demonstrate the presented algorithms. The results obtained can be applied to the geometric design or parameter (leg length) setup of this type of parallel robots.

Although this work uses the MSSM architecture for demonstration, the presented algorithm does not lose generality and can be applied to any type of Gough–Stewart platforms.

## Acknowledgements

The authors would like to acknowledge the financial support of the Natural Sciences and Engineering Research Council of Canada (NSERC) as well as the Canada Research Chair (CRC) Program.

## References

- [1] C. Gosselin, J. Angeles, Singularity analysis of closed-loop kinematic chains, *IEEE Transactions on Robotics and Automation* 6 (3) (1990) 281–290.
- [2] D. Zlatanov, R.G. Fenton, B. Behhabid, Singularity analysis of mechanisms and robots via a velocity-equation model of the instantaneous kinematics, in: Proceedings of the IEEE International Conference on Robotics and Automation, San Diego, CA, USA, 1994, pp. 986–991.
- [3] C.L. Collins, J.M. McCarthy, The quartic singularity surfaces of planar platforms in the Clifford algebra of the projective plane, *Mechanism and Machine Theory* 33 (7) (1998) 931–944.
- [4] S. Bhattacharya, H. Hatwal, A. Ghosh, Comparison of an xExact and an approximate method of singularity avoidance in platform type parallel manipulators, *Mechanism and Machine Theory* 33 (7) (1998) 965–974.
- [5] A.K. Dash, I.M. Chen, S.H. Yeo, G. Yang, Singularity-free path planning of parallel manipulators using clustering algorithm and line geometry, in: ICRA-2003, 2003.
- [6] S. Sen, B. Dasgupta, A.K. Mallik, Variational approach for singularity-free path-planning of parallel manipulators, *Mechanism and Machine Theory* 38 (11) (2003) 1165–1183.
- [7] K.H. Hunt, P.R. McAree, The octahedral manipulator: geometry and mobility, *International Journal of Robotics Research* 17 (8) (1998) 868–885.
- [8] B. Mayer St-Onge, C. Gosselin, Singularity analysis and representation of the general Gough–Stewart platform, *International Journal of Robotics Research* 19 (3) (2000) 271–288.
- [9] J.P. Merlet, D. Daney, A formal-numerical approach to determine the presence of singularity within the workspace of a parallel robot, in: Proceedings of the International Workshop on Computational Kinematics, Seoul, May 20–22, 2001, pp. 167–176.
- [10] H. Li, C. Gosselin, M. Richard, Determination of the maximal singularity-free zones in the six-dimensional workspace of the general Gough–Stewart platform, *Mechanism and Machine Theory* 42 (4) (2007) 497–511.
- [11] E.F. Fichter, A Stewart platform-based manipulator: general theory and practical construction, *International Journal of Robotics Research* 5 (2) (1986) 157–182.
- [12] C. Gosselin, Determination of the workspace of 6-DOF parallel manipulators, *ASME Journal of Mechanical Design* 112 (1990) 331–336.
- [13] J.P. Merlet, Trajectory verification in the workspace for parallel manipulator, *International Journal of Robotics Research* 13 (4) (1994) 326–333.
- [14] P.R. McAree, R.W. Daniel, An explanation of never-special assembly changing motions for 3-3 parallel manipulators, *International Journal of Robotics Research* 18 (6) (1999) 556–574.
- [15] J.P. Merlet, Determination of 6D workspaces of Gough-type parallel manipulator and comparison between different geometries, *International Journal of Robotics Research* 18 (9) (1999) 902–916.
- [16] F. Pernkopf, M. Husty, Workspace analysis of Stewart–Gough-type parallel manipulators, *Proceedings of the I MECH E Part C: Journal of Mechanical Engineering Science* 220 (7) (2006) 1019–1032.
- [17] I.A. Bonev, D. Zlatanov, C. Gosselin, Advantages of the modified Euler angles in the design and control of PKMs, in: Proceeding of the Third Chemnitz Parallel Kinematics Seminar, Parallel Kinematic Machines International Conference, Chemnitz, Germany, April 23–25, 2002, pp. 171–187.
- [18] L. Romdhane, Orientation workspace of fully parallel mechanisms, *European Journal of Mechanics (A/Solids)* 13 (4) (1994) 541–553.
- [19] J.P. Merlet, Determination of the orientation workspace of parallel manipulators, *Journal of Intelligent and Robotic Systems* 13 (1995) 143–160.
- [20] I. Bonev, J. Ryu, A new approach to orientation workspace analysis of 6-DOF parallel manipulators, *Mechanism and Machine Theory* 36 (2001) 15–28.
- [21] S.H. Lee, J.B. Song, W.C. Choi, D. Hong, Workspace and force–moment transmission of a variable arm type parallel manipulator, in: Proceedings of the 2002 IEEE International Conference on Robotics & Automation, Washington, DC, 2002, pp. 3666–3671.
- [22] G. Yang, W. Lin, S.K. Mustafa, I.M. Chen, S.H. Yeo, Numerical orientation workspace analysis with different parameterization methods, in: IEEE Conference on Robotics, Automation and Mechatronics, Bangkok, Thailand, 2006.
- [23] G.L. Yang, H.L. Ho, W. Lin, I.M. Chen, A differential geometry approach for the workspace analysis of spherical parallel manipulators, in: 11th World Congress in Mechanism and Machine Science, Tianjin, China, vol. 4, 1–4 April, 2004, pp. 2060–2065.